International Journal of Heat and Mass Transfer 52 (2009) 851–859

Contents lists available at ScienceDirect

International Journal of Heat and Mass Transfer

journal homepage: www.elsevier.com/locate/ijhmt

Numerical heat transfer analysis of encapsulated ice thermal energy storage system with variable heat transfer coefficient in downstream

Aytunc Erek [a,1], Ibrahim Dincer [b,*]

[a] Department of Mechanical Engineering, Dokuz Eylul University, Izmir, Turkey
[b] Faculty of Engineering and Applied Science, University of Ontario Institute of Technology, 2000 Simcoe Street North, Oshawa, Ont., Canada L1H 7K4

ARTICLE INFO

Article history:
Received 30 October 2007
Received in revised form 27 June 2008
Available online 11 September 2008

Keywords:
Heat transfer
Phase change
Solidification
Phase change
Encapsulated ice
Energy storage

ABSTRACT

During charging and discharging processes, the heat transfer behavior of the encapsulated ice thermal energy storage (TES) system changes during downstream case and this should be taken into account since the temperature of heat transfer fluid (HTF) and especially the heat transfer coefficient varies considerably around each capsule. This requires a careful study of the problem with variable heat transfer coefficient to contribute to the state-of-the-art. This has been the primary motivation behind the present study. Here, we first develop a new heat transfer coefficient correlation by simulating a series of 120 numerical experiments for different capsule diameters, mass flow rates and temperatures of HTF and second undertake a comprehensive numerical analysis using the temperature based fixed grid solution with control volume approach for studying the heat transfer behavior of an encapsulated ice TES system. Thirdly, we validate the present numerical model and the new correlation with some experimental data obtained from the literature, and hence a good agreement is obtained between the model results and experimental data. The results indicate that the heat transfer coefficient varies greatly during downstream and highly affects the heat transfer taking place during the process. So, the solutions with constant heat transfer coefficient appear to be unreliable for analysis and system optimization. The results also show that the solidification process is chiefly governed by the magnitude of Stefan number, capsule diameter and capsule row number.

1. Introduction

Thermal energy storage (TES) can not only play a significant role in shifting cooling loads in buildings by reducing demand for electrical power for air conditioning or cooling system during times of peak power usage, but energy costs can also be reduced by shifting the cooling load to off-peak hours when cheaper electricity is available. Reduction of this energy costs can be saved in several ways, compared to conventional chillers. First, at nighttime chiller operation takes advantage of lower temperatures relative to daytime values, which also reduce chiller lift. Second, the base-load power plants that operate at night typically have higher electricity generation efficiencies than the plants brought on-line to meet peak electricity demand. Furthermore, electricity transmission and distribution losses typically are higher during peak demand periods than during the night.

TES systems may take place either as a static process, in which heat transfer takes place via a solid surface, or a dynamic process, in which the heat transfer medium and storage medium are in direct contact. External and internal melt ice-on-coil and encapsulated ice storage systems belong to the group of static process. Ice slurry and ice-harvesting storage systems are of dynamic processes. In the case of a static process ice storage system, as the storage is charged, a layer of ice builds on the heat transfer surface. The layer essentially increases the resistance to heat transfer, which causes the evaporating temperature to fall and results in a reduced coefficient of performance for the chiller. This problem may be avoided in dynamic process ice storage systems because the ice is periodically or continually removed and there is no ice layer on the surface for a long time. Out of all the static TES systems, the encapsulated ice storage systems appear to be more effective and simpler because of providing the larger heat transfer area per unit storage volume, resulting in higher and faster heat transfer rate. The phenomenon of the phase change that takes place inside the PCM capsules of the latent TES system in TES applications is the primary interest of the present research work.

In the literature many researchers e.g., [1–13] have undertaken various studies to investigate such latent TES systems. Tao [1] presented a numerical method for the solidification problem inside both cylindrical and spherical containers. In his model, the heat capacity and thermal conductivity of solid region and heat transfer coefficient are assumed to be constant. Shih and Chou [2]

* Corresponding author. Tel.: +1 905 721 8668; fax: +1 905 721 3370.
E-mail address: ibrahim.dincer@uoit.ca (I. Dincer).
[1] Currently on his sabbatical leave at University of Ontario Institute of Technology.

0017-9310/$ - see front matter © 2008 Elsevier Ltd. All rights reserved.
doi:10.1016/j.ijheatmasstransfer.2008.06.024

Nomenclature

c, c_p	specific heat, J/kg K
C^0	$c^* \rho$, heat capacity, J/m^3.K
C	$C^0/(c_l \rho_l)$
C_{sl}	c_s/c_l
D	capsule outer diameter, m
Fo	$\alpha_f t/D^2$, Fourier number
h	enthalpy, J/kg
H	dimensionless enthalpy
HTF	heat transfer fluid
k	thermal conductivity, W/m.K
K	k/k_l, dimensionless thermal conductivity
K_{sl}	k_s/k_l
$\dot{m}$	mass flow rate, kg/s
Nu	Nusselt number
PCM	phase change material
Pe_f	$Re_f Pr_f$, fluid Peclet number
Pr_f	ν_f/α_f, fluid Prandtl number
q^0	heat transfer rate, W
q	$q^0/(\alpha_l . \Delta H D)$, dimensionless heat transfer rate
Q^0	total stored energy, J
Q	$Q^0/(\Delta H D^3)$, dimensionless total stored energy
r	radial coordinate, m
R	r/D, dimensionless radial direction
R_i	dimensionless inner radius
Re_f	$\rho.u.D/\mu$, fluid Reynolds number
S^0	source term
S	$S^0/\rho_l c_l (T_m - T_{in})$, dimensionless source term
Ste	$\rho_s.c_s(T_m - T_{in})/\Delta H$, Stefan number
t	time, s
t_w	$\frac{(D-D_i)}{2D}$dimensionless wall thickness of capsules
T	temperature, °C
TES	thermal energy storage
X	x/D, dimensionless axial direction

Greek symbols

α	thermal diffusivity, m^2/s
$\delta\theta_m$	$\delta T_m/(T_m - T_{in})$
ΔH	latent heat of PCM, J/m^3
θ	$(T - T_m)/(T_m - T_{in})$, dimensionless temperature
μ	dynamic viscosity, N s/m
ρ	density, kg/m^3
τ	$\alpha_f t/D^2$, dimensionless time
ν	kinematic viscosity, m^2/s

Subscripts

f	transfer fluid
i	initial condition
inf	outside of the thermal storage tank
in	inlet
l	liquid PCM
m	mushy phase
s	solid PCM or inner surface
w	container wall or surface

developed an iterative method for solidification process in spherical capsules. Chen and Yue [3] developed a 1-D porous medium model to estimate the thermal characteristics of ice-water cool storage in packed capsules for air conditioning. Comparisons of this theory with experimental data of temperature profiles of PCM (water) and coolant (ethyl alcohol) for various porosities, flow rates and different inlet coolant temperatures showed somewhat good agreement. Eames and Adref [4] studied experimentally the characteristics of heat transfer for water contained in spherical elements in both charging and discharging processes and described a novel method to measure interface position during solidification. Ismail and Henriquez [5] applied a finite-difference approximation and moving grid approach to solidification problem inside spherical container. Ismail et al. [6] presented some numerical results on the heat transfer during solidification process of water inside a spherical nodule. In their study, the effect of the size and material of container and flow parameters on solidification time and solidification rate were discussed. Bilir and Ilken [7] investigated numerically the inward solidification problem of a phase change material encapsulated in a cylindrical/spherical container with a third kind of boundary condition and ended up with a correlation which express the dimensionless total solidification time in terms of Stefan number, Biot number and superheat parameter. Rosen et al. [8] presented a thermodynamic performance model for an encapsulated ice thermal energy storage system using energy and exergy analyses. Their results indicated that energy analysis leads to misleadingly optimistic statement of TES efficiency and that exergy analysis is required for better analysis, design, optimization, and performance improvement. The heat transfer characteristics of the phase change process inside a horizontal cylindrical capsule for paraffin wax as PCM were investigated numerically and experimentally by Ref. [9]. Their results indicated that the melting process is chiefly governed by the magnitude of the Stefan number.

Encapsulated containers are subject to super cooling effect, i.e., cooling of the liquid water inside the container below its freezing point prior to the ice formation. Supercooling may occur only in fully discharged containers and result in a reduced rate of heat transfer at the beginning of the charging process. Supercooling may be significantly reduced by the addition of nucleating agents. Bedecarrats et al. [10] realized a model taking into account the supercooling phenomenon and were investigated experimentally and numerically the process of energy storage in a tank randomly filled with PCM encapsulated in spherical capsules. Kousksou et al. [11] presented the influences of the position of the storage tank and the flow pattern inside the tank included spherical capsules by using two dimensional porous-medium approach. Chen et al. [12] studied experimentally the nucleation probability of supercooled water inside capsules and investigated the effect of different macrofactors on the nucleation behavior of capsules. In another work about cold storage in an encapsulated system, Chen et al. [13] presented the thermal behavior of TES system during charging process with varying inlet coolant temperature and coolant flow rate. The study by Cho and Choi [14] include the thermal characteristics of paraffin wax in a spherical capsule during freezing and melting processes. They found out that the average heat transfer coefficient around capsules were affected by the inlet and initial temperature and Reynolds number more during the melting process than the freezing process due to a natural-convection effect during the melting process.

To the best of the authors' knowledge, in the open literature the use of an average heat transfer coefficient for heat transfer analysis (either analytical or numerical) in the encapsulated ice TES systems is a common approach. In most instances the model results deviate drastically compared to experimental data/findings. This has been a primary motive behind the present work to develop a new heat transfer coefficient correlation by simulating a series of 120 numerical experiments for different capsule diameters, mass

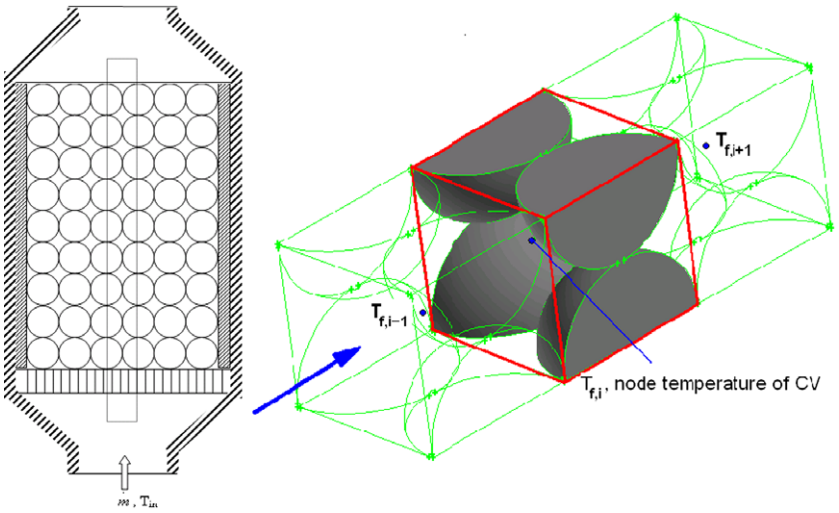

Fig. 1. Schematic view of physical model and mathematical model.

flow rates and temperatures of heat transfer fluid and study the heat transfer in an encapsulated ice TES system as shown in Fig. 1 and the heat transfer behavior in downstream, and compare the model results with some experimental data.

2. Modeling

As illustrated in Fig. 1a, the thermal energy storage system consists of a cylindrical tank of height H and diameter of D_{inf} and spherical capsules containing PCM which is in it. In this study, only charging process is studied and thermal behavior of TES system is investigated numerically. In the charging process, the cold heat transfer fluid flows on capsules and the PCM in capsules solidify toward the center with time. The following assumptions are considered in numerical model:

- The PCM is homogenous and isentropic.
- The tank is completely insulated.
- The temperature in the tank dominantly changes only along axial direction with time.
- The heat transfer mechanism inside container is only dominated by conduction in radial direction.
- The heat flux is isotropic on the whole PCM capsule area.
- The effect of natural convection in tank neglects.
- The thermophysical properties of container wall and HTF are independent of temperature, but the properties of PCM are considered different in the solid and liquid phases. The pure water is taken as the PCM in the parametric study.

Since the numerical analysis of such a three-dimensional and time dependent system is difficult to be modeled, it is sufficient to simplify system is using symmetry surfaces and the system that include four quarter spherical capsules and heat transfer fluid around them, as shown Fig. 1b. A three-dimensional view considered in the numerical study for an encapsulated ice system is also shown in Fig. 1(b). Assuming that the heat loss from the system is negligible, the heat transfer equation of the heat transfer fluid can be expressed as

$$\varepsilon\rho_f c_f \frac{\partial T_f}{\partial t} + \rho_f c_f u \frac{\partial T_f}{\partial x} = \frac{\partial}{\partial x}\left(\varepsilon\, k_f \frac{\partial T_f}{\partial x}\right) + q^0_{capsule}/V_{CV} \quad (1)$$

where $q^0_{capsule}$ represents the heat transfer from capsules to HTF. As seen Fig. 1b, the fluid around four quarter capsules is taken as control volume. The reason is that the discretization of Eq. (1) is easy and the assumption of constant surface temperature and temperature distribution with only radial direction will have realized due to assumption of the dimensional heat conduction inside capsules. The heat transfer between the HTF and PCM inside capsules can be determined using the following analogy:

$$q^0_{capsule} = \frac{T_{s,i} - T_{f,i}}{R_{t,cond} + R_{t,conv}} \quad (2)$$

where $R_{t,\,cond}$ and $R_{t,conv}$ represent thermal conduction and convection resistance, respectively. After rearranging the terms, it can be written as

$$q^0_{capsule} = (T_{s,i} - T_{f,i}) \Big/ \frac{1}{h.\pi D^2} + \frac{1}{2\pi k}\left(\frac{1}{D_i} - \frac{1}{D}\right) \quad (3)$$

Rewriting Eq. (1) in the dimensionless form,

$$\varepsilon.C_f \frac{\partial \theta_f}{\partial Fo} + C_f Re_f \cdot Pr_f \frac{\partial \theta_f}{\partial X} = \frac{\alpha_l}{\alpha_f}\frac{\partial}{\partial X}\left(\varepsilon \cdot K_f \frac{\partial \theta_f}{\partial X}\right) + \frac{q'''_{capsule}}{D \cdot k_f (T_m - T_{in})} \quad (4)$$

The dimensionless heat transfer can then be written as

$$q_{capsule} = \pi.(\theta_{s,i} - \theta_{f,i}) \Big/ \frac{1}{Nu_f} + \frac{K_f}{K_w}\left(\frac{t_w}{1 - 2t_w}\right) \quad (5)$$

Note that the relation between $q_{capsule}$ and $q^0_{capsule}$ is $q_{capsule} = q^0_{capsule}/D \cdot k_f(T_m - T_{in})$. In this study, heat transfer coefficient, Nu_f, is obtained from the CFD analysis. The details on numerical analysis are given in the next section.

In order to link in related to heat transfer between capsules and HTF using $q_{capsule}$, the heat transfer equation for the PCM capsules is required for solution. The heat transfer equation in the spherical capsules is described by a temperature transforming method using fixed grid numerical model [14,15]. In this method, it is assumed that phase change process occurs over a range of phase change temperature from $T_m - \delta T_m$ to $T_m + \delta T_m$, but it can also be successfully used to simulate solidification process occurring at a single temperature by taking a small range of phase change temperature, $2\delta T_m$. For the case where water is used as PCM, there is a quick transition from solid to liquid, and in this regard the value of dimensionless semi range phase-change temperature, $\delta\theta_m$, is taken as 0.001.

The dimensionless heat transfer equation for the PCM in the capsules is written as

$$\frac{\partial(C\theta)}{\partial Fo} = \frac{\alpha_l}{\alpha_f}\frac{1}{R^2}\frac{\partial}{\partial R}\left(KR^2\frac{\partial\theta}{\partial R}\right) - \frac{\partial S}{\partial \tau} \tag{6}$$

where

$$C = C(\theta) = \begin{cases} C_{sl} & \theta < -\delta\theta_m \quad \text{Solid} \\ \frac{1}{2}(1+C_{sl}) + \frac{C_{sl}}{2Ste\delta\theta_m} & -\delta\theta_m \leqslant \theta \leqslant \delta\theta_m \quad \text{Mushy} \\ 1 & \theta > \delta\theta_m \quad \text{Liquid} \end{cases} \tag{7}$$

$$S = S(\theta) = \begin{cases} C_{sl}\delta\theta_m & \theta < -\delta\theta_m \quad \text{Solid} \\ \frac{1}{2}\delta\theta_m(1+C_{sl}) + \frac{C_{sl}}{2Ste} & -\delta\theta_m \leqslant \theta \leqslant \delta\theta_m \quad \text{Mushy} \\ C_{sl}\delta\theta_m + \frac{C_{sl}}{Ste} & \theta > \delta\theta_m \quad \text{Liquid} \end{cases} \tag{8}$$

$$K = K(\theta) = \begin{cases} K_{sl} & \theta < -\delta\theta_m \quad \text{Solid} \\ K_{sl} + \frac{(1-K_{sl})(\theta+\delta\theta_m)}{2\delta\theta_m} & -\delta\theta_m \leqslant \theta \leqslant \delta\theta_m \quad \text{Mushy} \\ 1 & \theta > \delta\theta_m \quad \text{Liquid} \end{cases} \tag{9}$$

The initial and boundary conditions are the written as follows:

- Initial condition (Fo = 0):

$$\text{At } 0 \leqslant R \leqslant R_i \rightarrow \theta = \theta_I \tag{10}$$

- Boundary conditions (Fo > 0):

$$\text{At } R = 0 \rightarrow \frac{\partial\theta}{\partial R} = 0 \tag{11}$$

$$\text{At } R = R_i \rightarrow -K\left(\frac{\partial\theta}{\partial R}\right)_{R=R_i} = q''_{capsule} \tag{12}$$

In case of studying of solidification process inside capsule, there are four stages for phase change process of water inside capsule [e.g., 12,13]. The first stage, called the sensible heat extraction process, is the process from initial stage to the subcooling state before water nucleation occurs. The second stage, called the dendritic ice formulation process, is the process from the form of nucleation to finishing of dendritic ice formulation. Other two stages are the processes of latent heat transfer and sensible heat transfer of solid, respectively. Since the interval of second stage relatively is very short as a time and modeling of this stage is difficult, in this study, the growth of ice crystal is not taken into account and the first two stages are combined into one, called sensible heat extraction process of liquid water.

Actually, the one dimensional conduction equation is written for the PCM inside a capsule, and the effect of natural convection that takes place inside the encapsulated liquid PCM is taken into account using an effective thermal conductivity given by [16]. The effective thermal conductivity is defined as

$$K_{effective} = \frac{Nu}{Nu_{cond}} \tag{13}$$

where $K_{effective}$ denotes the ratio of total heat transfer rate to heat transfer rate by conduction.

The current literature indicates that a limited number of studies are about the natural convection number inside the encapsulated PCM. Here, the Nusselt number correlated experimentally by Ettouney et al. [17] for the capsule during melting and solidification is used in the present study.

The temperature distribution inside the solution domain is calculated by solving the heat transfer equations defined through Eqs. (4)–(9). The solution procedure used for solving these energy equations is a control-volume approach as described by e.g., [18]. On the other hand, the thermal conductivity, K, is calculated by a harmonic mean method at the control surface, and the thermal conductivity for any control surface, K_n, results in

$$K_n = 1\Big/\frac{1-f_n}{K_P} + \frac{f_n}{K_N} \tag{14}$$

where the interpolation factor, f_n, is defined as

$$f_n = \frac{1}{R_n} - \frac{1}{R_N}\Big/\frac{1}{R_P} - \frac{1}{R_N} \tag{15}$$

where P and N denote control volume nodes and n denotes control surface.

Here, the semi implicit solver, [19], is used for solving the discretization equations of heat transfer equations. Using this solver, the CPU time is reduced a great amount for a single iteration and this solver requires the less storage than the other solvers such as Gauss–Seidel iteration method. Since the energy equation for the PCM is a non-linear heat conduction equation, iterations are needed during each time step. For a given time step, convergence is declared at the $k+1$th iteration when $\left|\theta_{i,j}^{k+1} - \theta_{i,j}^{k}\right| \leqslant 10^{-6}$. The numerical results are then verified by testing the resulting predictions for independence of the grid size, time-step and other parameters. The grid size used for the solution was 200 (radial) for each capsule with a time step $\Delta t = 0.1$ s. Furthermore, the overall energy balance is checked during the calculation process to verify the numerical results. At a time step, the change heat storage in PCM and container wall must be equal to the total energy supplied by the heat transfer fluid as follows,

$$\int_0^\tau Pe_f \cdot C_f \cdot (\theta_{b,out} + 1) \cdot d\tau = \sum_{k=1}^{N}\int_{R=0}^{R_i} 4\pi \cdot R \cdot (H - H_i) \cdot dR \tag{16}$$

where $H = C \times T + S$ stands for total enthalpy at the control volume. The left side of the Eq. 16 represents the thermal energy supplied by the heat transfer fluid and the right side of equation represents the thermal stored energy in the encapsulated PCM. In calculation procedure, the numerical deviation between two sides of Eq. 16 is taken less than 1%.

3. Calculation of heat transfer coefficient around spherical capsules

As mentioned before, the heat transfer coefficient changes along flow since the fluid flow around capsules is not hydrodynamically and thermally developed. However, the changes in the heat transfer coefficient along flow line were not taken into account in the previous studies, and the use of an average heat transfer coefficient was common for analyzing the encapsulated TES. In this section, we study the variation of heat transfer coefficient. A schematic view of the physical model is shown in Fig. 1a. Due to the difficulties of modeling and analyzing of whole thermal energy storage system shown in Fig. 1a, the model is rather simplified as Fig. 1b by considering flows around capsules and taking symmetry planes. The heat transfer fluid flows four quarter spherical capsules which are kept at constant temperature of 273.15 K for each segment. The side walls are taken symmetric planes on account of natural of physical phenomenon. At the inlet, fluid with constant mass flow rate $\dot{m}$ and temperature T_{in} enters the TES system at a constant speed of u_0. The flow is assumed to be developing and steady. Here, ethylalcohol is taken as HTF in order to compare the results obtained from numerical analysis with the experimental data performed by Chen and Yue [3]. In the calculation of the heat transfer coefficient, the density, thermal conductivity and dynamic viscosity of the HTF are taken linear and second order polynomial depending on temperature. The thermophysical properties of HTF are given as Table 1. The primitive volume mesh for the FLUENT computational fluid dynamics program used to obtain solutions

Table 1
Thermophysical properties of HTF, capsule wall and PCM

Material	Temperature or phase	ρ (kg m^{-3})	c_p (J kg^{-1} K^{-1})	k (W m^{-1} K^{-1})	α (m^2 s^{-1})	μ (Pa s)	ΔH (J m^{-3})
HTF (ethyl alcohol)	−10 °C	838.594	2252.917		$1.053^{*}10^{-7}$	0.0030	–
	−15 °C	842.940	2208.537	0.199	$1.069^{*}10^{-7}$	0.0034	–
	−20 °C	847.286	2148.665		$1.093^{*}10^{-7}$	0.0038	–
HTF (ethylene glycol 40%)	−5 °C	1068.28	3384	0.389	$1.08^{*}10^{-7}$	$7.18^{*}10^{-3}$	–
	−10 °C	1069.63	3367	0.383	$1.06^{*}10^{-7}$	$9.06^{*}10^{-3}$	–
	−15 °C	1070.87	3351	0.377	$1.05^{*}10^{-7}$	$11.74^{*}10^{-3}$	–
Capsule wall (polyethylene)		940	1900	0.35	$1.96^{*}10^{-7}$	–	–
PCM (*n*-tetradecane)	Liquid	765	2100	0.211	$1.31^{*}10^{-7}$	–	$175.2^{*}10^{6}$
	Solid	803	1800	0.273	–	–	
PCM (water)	Liquid	999.8	4217	0.561	$1.33^{*}10^{-7}$	–	$333.5^{*}10^{6}$
	Solid	916.8	2040	2.2	–	–	

was constructed with the aid of the GAMBIT program. Along the entire system, 20 separate zones for each capsule zone and additional two zones for inlet and outlet, in order to specify uniform velocity for inlet and outflow for outlet, are formed as illustrated in Fig. 1b. For each simulation, nearly 650,000 tetrahedral cells are used.

For the HTF, the following are the basic conservation equations of continuity, momentum and energy:

$$\frac{\partial}{\partial x_i}(\rho u_i) = 0, \quad \frac{\partial}{\partial x_i}(\rho u_i u_j) = -\frac{\partial P}{\partial x_i} + \frac{\partial \tau_{ij}}{\partial x_j} + \rho g_i + S_i, \quad \text{and} \quad \frac{\partial}{\partial x_i}(\rho u_i h) = \frac{\partial}{\partial x_i}\left(k\frac{\partial T}{\partial x_i}\right)$$

where ρ is density, u_i is the velocity component in the i direction, p is the static pressure, x_i is a cartesian coordinate, τ_{ij} is the stress tensor, g_i is the gravitation acceleration in the i direction, k is thermal conductivity, T is temperature, and t is time. In this study the viscous heating term is not taken into accounts since it is negligibly small.

The numerical solution is done using the Fluent 6.0 software. The governing equations for flow and heat transfer in internal flow around spherical capsules are solved with the control–volume method introduced by Patankar [18]. The SIMPLEC algorithm offered by Doormal and Raithby [20] is used to resolve the coupling between velocity and pressure.

4. Results and discussion

The first objective of this study is to investigate the variation of the heat transfer coefficient around the spherical capsules with flow line in downstream. For this purpose, a three-dimensional model as shown in Fig. 1b was created for four different capsule diameter (D = 40, 60, 70 and 80 mm) with the same wall thickness of 1 mm. Here we focus on heat transfer coefficient around capsules, so the surface temperature of capsules is taken as constant as a result of the heat transfer fluid around capsules. After forming the models, a series of 120 numerical experiments were performed to calculate the heat transfer coefficient for different capsule diameter, mass flow rate, and inlet temperature of HTF and especially for different capsule layers as summarized in Tables 2 and 3. Although all datasets are available, the numerical results for capsule diameters of

Table 2
The numerical obtained experimental parameters and the heat transfer coefficient values for a capsule outer diameter value of 40 mm at various capsule rows

Mass flowrate, kg/s	Inlet temp., K	Heat transfer coefficients [W/m^2 K]							
		Capsule 1	Capsule 2	Capsule 3	Capsule 4	Capsule 5	Capsule 10	Capsule 15	Capsule 20
0.003	268.15	59.65	36.20	32.19	28.81	26.33	16.49	10.49	7.56
0.003	265.65	89.12	54.23	48.22	43.14	39.42	24.69	15.71	11.32
0.003	263.15	118.32	72.18	64.17	57.38	52.43	32.84	20.89	15.05
0.003	260.65	147.24	90.03	80.00	71.52	65.33	40.92	26.03	18.75
0.003	258.15	175.85	107.74	95.70	85.51	78.11	48.92	31.12	22.41
0.003	253.15	232.04	142.64	126.56	113.00	103.17	64.61	41.09	29.58
0.005	268.15	76.18	50.59	45.92	41.96	39.07	26.76	18.59	14.66
0.005	265.65	113.75	75.64	68.70	62.78	58.46	40.07	27.84	21.96
0.005	263.15	150.97	100.48	91.31	83.45	77.72	53.28	37.04	29.22
0.005	260.65	142.44	125.09	113.73	103.94	96.80	66.39	46.17	36.43
0.005	258.15	224.21	149.44	135.92	124.22	115.68	79.37	55.21	43.58
0.005	253.15	295.68	197.25	179.47	164.00	152.70	104.82	72.95	57.59
0.0075	268.15	89.83	63.95	58.95	54.67	51.59	37.82	28.04	23.50
0.0075	265.65	134.16	95.56	88.16	81.77	77.18	60.30	41.98	35.20
0.0075	263.15	178.09	126.89	117.13	108.68	102.58	75.26	55.84	46.84
0.0075	260.65	230.23	164.07	151.55	140.65	132.76	97.44	72.32	60.69
0.0075	258.15	264.77	188.64	174.29	161.74	152.67	112.06	83.18	69.78
0.0075	253.15	349.38	248.83	230.05	213.54	201.55	147.96	109.87	92.23
0.01	268.15	99.53	74.08	68.99	64.62	61.50	47.17	36.52	31.76
0.01	265.65	148.65	110.64	103.13	96.63	91.97	70.59	54.67	47.57
0.01	263.15	197.33	146.87	137.01	128.41	122.22	93.83	72.69	62.61
0.01	260.65	245.56	182.74	170.57	159.90	152.20	116.87	90.57	78.90
0.01	258.15	293.32	218.23	203.79	191.07	181.88	139.66	108.27	94.19
0.01	253.15	387.29	287.87	269.01	252.27	240.13	184.36	142.96	124.54
0.05	268.15	151.28	134.39	131.98	128.91	126.55	115.48	105.60	98.75
0.05	265.65	226.06	200.31	196.64	192.14	188.65	172.19	157.64	147.98
0.05	263.15	300.22	265.36	260.48	254.54	249.94	228.26	209.11	196.10
0.05	260.65	373.74	329.60	323.46	316.14	310.41	283.63	259.93	244.59
0.05	258.15	446.62	393.02	385.66	376.89	370.11	338.24	310.09	292.27
0.05	253.15	590.39	517.57	507.63	495.96	487.04	445.13	408.28	384.99

Table 3
The numerical obtained experimental parameters and the heat transfer coefficient values for a capsule outer diameter value of 80 mm at various capsule rows

Mass flowrate, kg/s	Inlet temp., K	Heat Transfer Coefficients [W/m^2 K]							
		Capsule 1	Capsule 2	Capsule 3	Capsule 4	Capsule 5	Capsule 10	Capsule 15	Capsule 20
0.003	268.15	20.20	11.35	9.58	8.30	7.32	4.00	2.19	1.33
0.003	265.65	30.27	17.06	14.37	12.44	10.97	5.98	3.27	1.98
0.003	263.15	40.30	22.77	19.14	16.55	14.59	7.95	4.34	2.63
0.003	260.65	50.29	28.47	23.89	20.64	18.18	9.89	5.40	3.26
0.003	258.15	60.23	34.15	28.61	24.69	21.74	11.80	6.44	3.89
0.003	253.15	79.88	45.39	37.91	32.66	28.72	15.55	8.47	5.10
0.005	268.15	26.92	16.18	14.05	12.52	11.29	6.89	4.21	2.92
0.005	265.65	40.23	24.27	21.06	18.75	16.90	10.31	6.30	4.37
0.005	263.15	53.45	32.33	28.04	24.94	22.48	13.70	8.37	5.81
0.005	260.65	66.54	40.36	34.97	31.09	28.02	17.07	10.42	7.23
0.005	258.15	79.51	48.33	41.85	37.18	33.51	20.41	12.46	8.64
0.005	253.15	105.01	64.05	55.39	49.15	44.28	26.94	16.44	11.40
0.0075	268.15	33.17	21.30	18.82	17.09	15.66	10.28	6.76	5.07
0.0075	265.65	49.54	31.88	28.18	25.59	23.44	15.39	10.12	7.59
0.0075	263.15	65.76	42.39	37.48	34.02	31.17	20.47	13.46	10.09
0.0075	260.65	81.81	52.83	46.71	42.38	38.83	25.51	16.78	12.58
0.0075	258.15	97.68	63.16	55.86	50.66	46.42	30.50	20.06	15.04
0.0075	253.15	128.84	83.50	73.83	66.90	61.29	40.28	26.50	19.87
0.01	268.15	37.90	25.61	22.85	21.04	19.48	13.43	9.26	7.29
0.01	265.65	56.60	38.29	34.19	31.47	29.14	20.11	13.87	10.92
0.01	263.15	75.12	50.87	45.46	41.83	38.74	26.74	18.45	14.53
0.01	260.65	93.45	63.33	56.63	52.09	48.25	33.32	23.00	18.12
0.01	258.15	111.58	75.66	67.69	62.24	57.66	39.83	27.50	21.67
0.01	253.15	147.15	99.88	89.42	82.16	76.11	52.60	36.34	28.64
0.05	268.15	65.19	55.26	51.96	50.26	48.75	42.11	36.26	33.30
0.05	265.65	97.28	82.32	77.44	74.94	72.71	62.88	54.18	49.88
0.05	263.15	129.05	109.05	102.60	99.33	96.39	83.44	71.92	66.34
0.05	260.65	160.51	135.43	127.45	123.44	119.81	103.76	89.48	82.73
0.05	258.15	191.66	161.50	152.01	147.26	142.95	123.85	106.82	98.90
0.05	253.15	253.04	212.63	200.22	194.01	188.35	163.20	140.78	130.64

40 mm and 80 mm only, in order to avoid duplicity, are tabulated in Tables 2 and 3. As can be seen from these tables, the heat transfer coefficient decreases dramatically with downstream. Furthermore, as the capsules diameter and inlet temperature (or temperature difference, $T_m - T_{in}$, decreases) increase and the mass flow rate decreases, the heat transfer coefficient decreases.

The velocity vectors along centerline are plotted in Fig. 2. The plot of velocity vectors shows clearly that flow characteristics around each capsule is different from another ones since the flow is developing. The heat transfer fluid comes in with uniform velocity to system and centerline velocity increases with downstream, like internal flow in channel. This situation is one argument of that

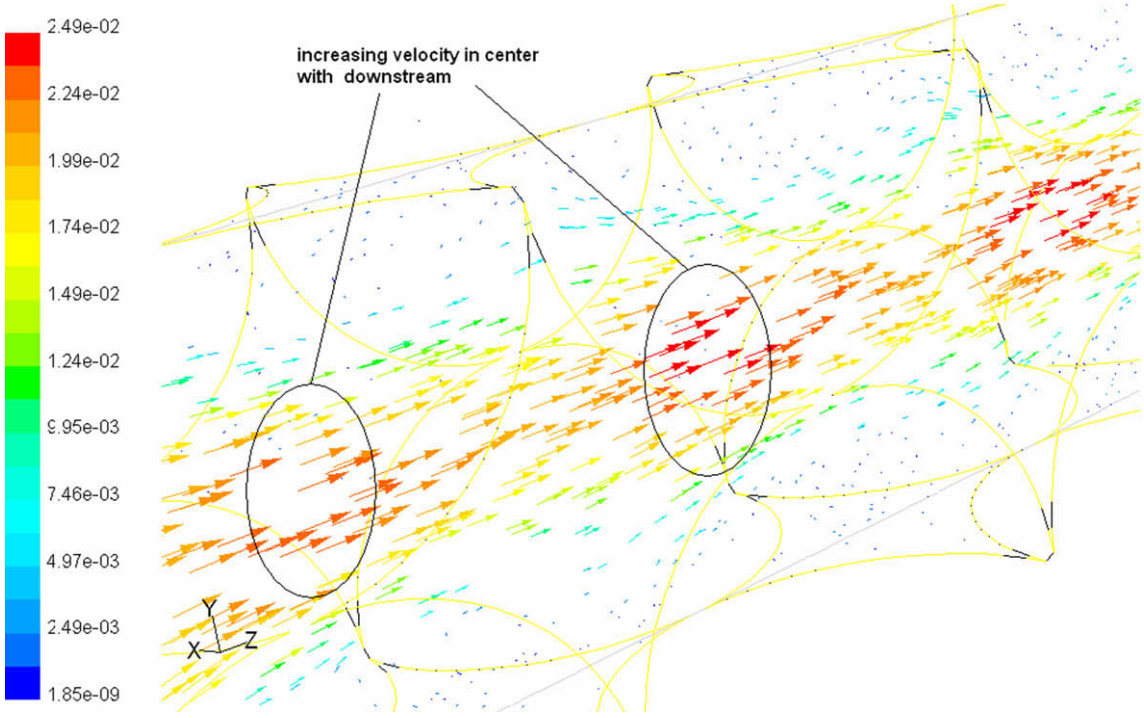

Fig. 2. Velocity vectors around the capsules.

the heat transfer coefficient will change with downstream as shown in Tables 2 and 3.

The key aspect of the present paper is to use a considerably high number of numerical datasets (e.g., 120) were used to correlate the heat transfer coefficient using the non linear regression method through SPSS 10. The heat transfer coefficient is the developed as

$$Nu_X = 0.726.(Re \cdot Pr)^{0.360}\left(\frac{T}{T_S}\right)^{-20.094} .X^{\frac{-450.656}{Re\,Pr}} \quad (17)$$

In this correlation, the correlation coefficient is obtained to be $R^2 = 0.950$. All the numerical experiment data and correlation curves plotted to show how much the present correlation agrees with the experimental data in Fig. 3. As shown in this figure, the correlation overlaps almost all numerical experiments data between two correlation curves which for $Pe = 500$ and $Pe = 15{,}000$. Since the power of axial direction is a function of the Peclet number, two correlation curves for different two Peclet numbers, which are lower and upper limit values for the numerical experiment data, are drawn in this figure. In addition to a high correlation coefficient, we go one step ahead and validate this correlation with some experimental data available in the literature [e.g., 3,21,22]. Chen and Yue [3] proposed a correlation based on experimental data and numerical results for heat transfer coefficient around spherical capsules. Note that Kunii and Suzuki [21] obtained the time-averaged internal heat transfer coefficients by matching the experimental measurements and theoretical results in temperature profile of coolant. Wakao et al. [22] corrected and correlated the published heat transfer data determined earlier studies for axial fluid thermal dispersion coefficients. The corrected data in the range of Reynolds number from 15 to 8500 are correlated by the analogous form of mass correlation. Fig. 4 shows the comparison of the heat transfer coefficient for the present our correlation and other studies [3,22]. It can be seen in this figure that agreement between these results is quite satisfactory. Having demonstrated the validity of the present correlation through comparisons with available correlation, the physical validity of the mathematical model should be made by comparison of predictions with experimental data. Cho and Choi [14] determined the temperature variations inside and on the surface of a spherical capsule filled with *n*-tetradecane located along centerline of the storage tank. In order to validate the numerical model with the experimental data from [14], the numerical code is tested for same geometrical and operational parameters and same PCM, HTF and container material; *n*-tetradecane, 40% aqueous solution of ethylene glycol and polyethylene, respectively; as given in Table 1. So, the comparison between numerical results and experimentally available data from [14] is given in Fig. 5. Although the present numerical model does not consider the sensible storage in the container wall, because of using electrical analogy in the numerical model, and does not include the supercooling phenomenon, there is still good agreement between the present numerical results and the experimental data employed. A sharp decrease in

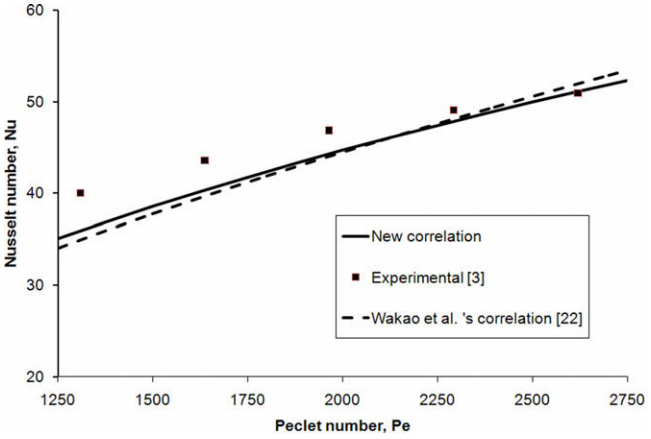

Fig. 4. Comparison between the present correlation and the experimental data from Ref. [3] and the literature correlation from Ref. [22].

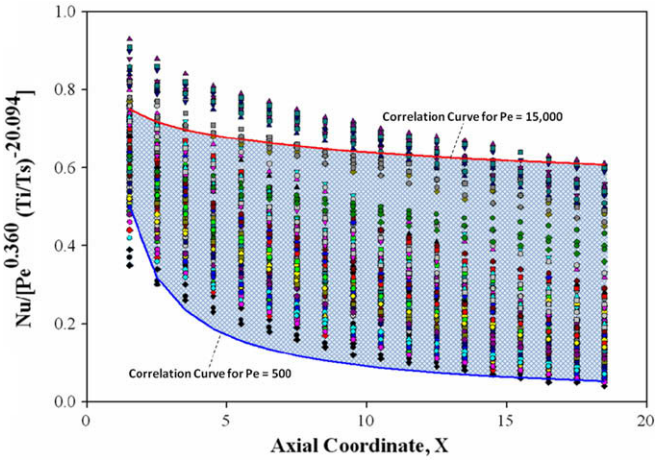

Fig. 3. Comparisons of the present heat transfer correlations with the numerical experiments data.

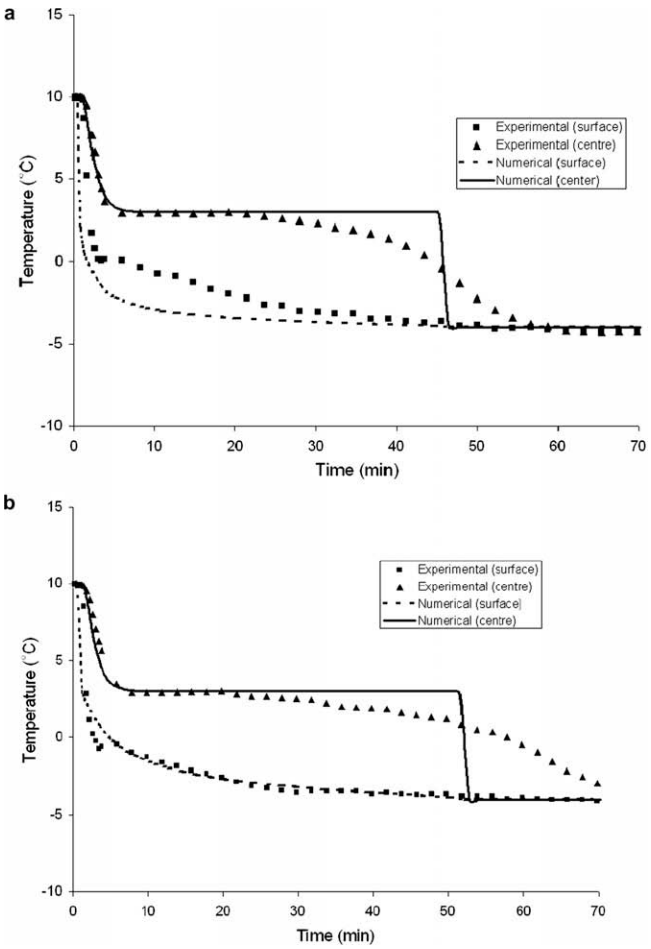

Fig. 5. Comparison between the numerical model and the experimental study. (a) for 1st layer, (b) for 7th layer.

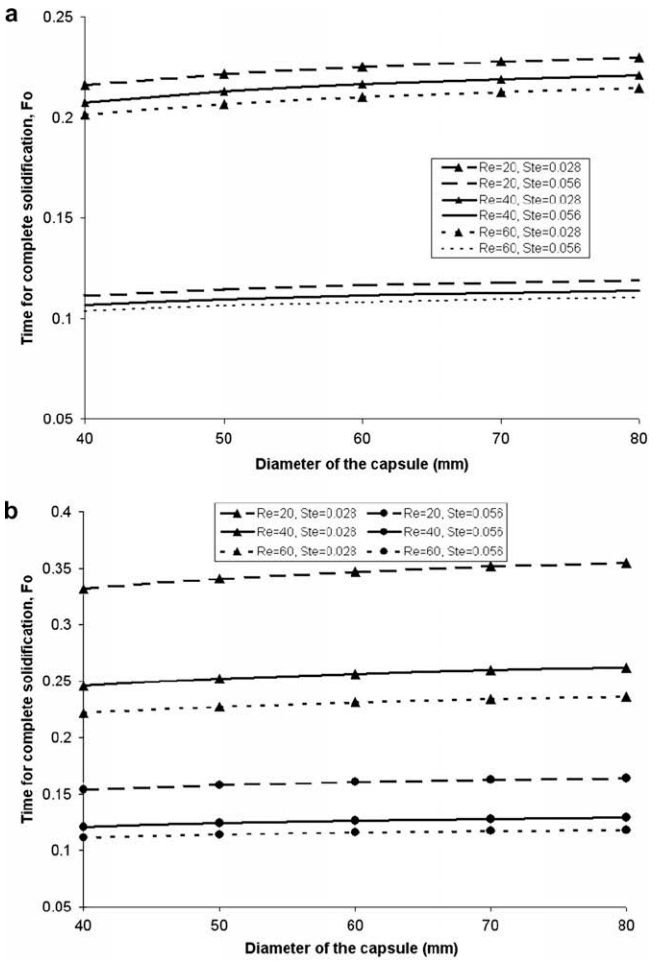

Fig. 6. Effect of Reynolds number and Stefan number on the time for complete solidification. (a) for 1st layer, (b) for 7th layer.

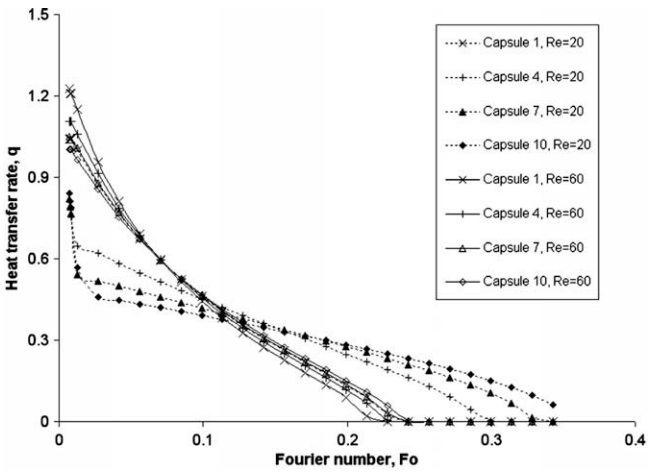

Fig. 7. Variation of heat transfer rate with Fourier number for different Reynolds numbers and capsule row numbers.

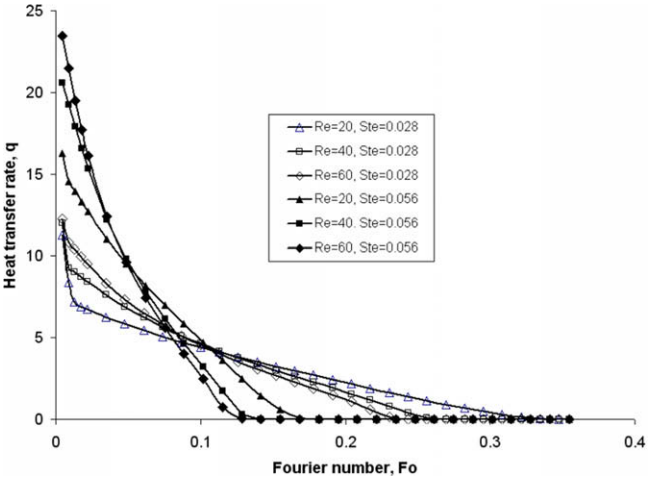

Fig. 8. Variation of heat transfer rate with Fourier number for different Reynolds numbers and Stefan numbers.

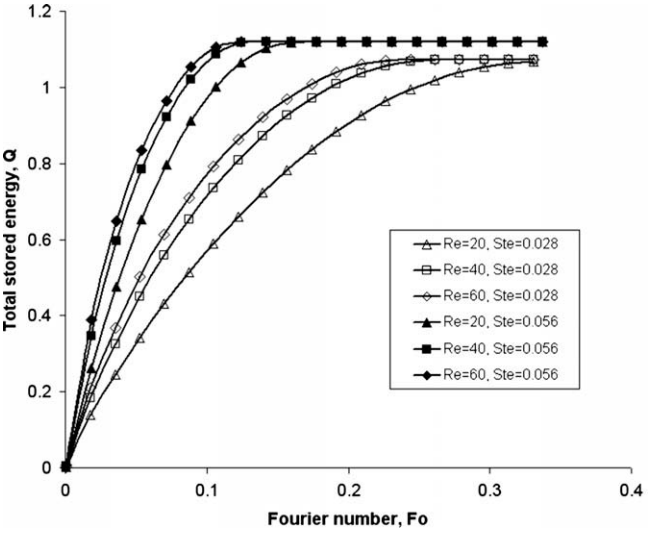

Fig. 9. Variation of total energy stored with Fourier number for different Reynolds numbers and Stefan numbers.

the centre temperature becomes more apparent as the nature of numerical analysis which reflects a similar situation as given in Ismail's works [5,6]. This situation occurs at the end of solidification process taken place.

The variation of the local heat transfer coefficient with downstream is very important as shown in Tables 2 and 3 and should take into account accordingly. The published literature confirms that the heat transfer coefficient was taken as constant on thermal analysis of the similar TES systems in the past all studies. Fig. 6 shows clearly why x-dependent heat transfer coefficient is so important. While Fig. 6a shows the variation of time for a complete solidification of each capsule for different Reynolds number and Stefan number at the first layer (or the first capsule), Fig 6b shows at seventh layers. While the solidification time is not sensitive to the change of Reynolds number for the first capsule, it becomes very sensitive and dependent in the seventh capsule. So, the effect of inlet HTF temperature or Stefan number on the solidification time is very sensitive for two cases. Though solidification time seems to not change with capsule diameter, it should be noted that this term is dimensionless time. But, it is an interesting result that the dimensionless solidification time does not change with capsule diameter.

The time dependent heat transfer rate on the different capsule layer for the case of $Re = 20$ and $Re = 60$ is shown in Fig. 7. As expected, the low Reynolds number makes more influence to the variation of the heat transfer rate with downstream than the higher Reynolds number. Namely the heat transfer rate does not change

with downstream for high Reynolds number. As a matter of fact, increasing Reynolds number increases the heat transfer rate.

Furthermore, the effect of Reynolds number and Stefan number on the heat transfer rate for a 60 mm of capsule diameter is illustrated in Fig. 8 as a representative case. The heat transfer rate increases as Reynolds number increases and inlet temperature of HTF decreases. But, the effect of Stefan number is more significant than that of Reynolds number.

Fig. 9 shows the total thermal heat stored as a function of time for different Reynolds numbers and Stefan number and a 60 mm of capsule diameter. The higher Reynolds number and Stefan number, the smaller total charging time. It should be noted that total stored heat increases with Stefan number at the end of charging process, since total sensible stored heat increases with the Stefan number.

5. Conclusions

In this study we have developed a new heat transfer coefficient correlation, using 120 datasets, with considering the change with downstream around a spherical capsule in a cold TES system and validated it with some experimental data available in the literature, resulting in considerably good agreement. In addition, a numerical analysis is carried out using a temperature based fixed grid solution with control volume approach for investigating the heat transfer behavior of an encapsulated ice TES system. The results show: (i) The effect of varying heat transfer coefficient on the heat transfer is crucial and must be considered for analysis. (ii) The heat transfer rate increases as Reynolds number increases and inlet temperature of HTF decreases. (iii) The solidification process is primarily governed by the magnitude of Stefan number, capsule diameter and capsule row number.

Acknowledgements

The authors acknowledge the support provided by Dokuz Eylul University in Turkey and the Natural Sciences and Engineering Research Council in Canada.

References

[1] L.C. Tao, Generalized numerical solutions of freezing a saturated liquid in cylinders and spheres, AIChE J. 13 (1) (1967) 165–169.
[2] Y.P. Shih, T.C. Chou, Analytical solutions for freezing a saturated liquid inside or outside sphere, Chem. Eng. Sci. 26 (1971) 1787–1793.
[3] S.L. Chen, J.S. Yue, Thermal performance of cool storage in packed capsules for air conditioning, Heat Recovery Syst. CHP 11 (1991) 551–561.
[4] I.W. Eames, K.T. Adref, Freezing and melting of water in spherical enclosures of the type used in thermal (ice) storage systems, Appl. Thermal Eng. 22 (2002) 733–745.
[5] K.A.R. Ismail, J.R. Henriquez, Solidification of PCM inside a spherical capsule, Energy Convers. Manag. 41 (2000) 173–187.
[6] K.A.R. Ismail, J.R. Henriquez, T.M. Silva, A parametric study on ice formation inside a spherical capsule, Int. J. Thermal Sci. 42 (2003) 881–887.
[7] L. Bilir, Z. İlken, Total solidification time of a liquid phase change material enclosed in cylindrical/spherical containers, Appl. Thermal Eng. 25 (2005) 1488–1502.
[8] M.A. Rosen, I. Dincer, N. Pedinelli, Thermodynamic performance of ice thermal energy storage systems, ASME J. Energy Resources Technol. 122 (2000) 205–211.
[9] A.F. Regin, S.C. Solanki, J.S. Saini, Latent heat thermal energy storage using cylindrical capsule: numerical and experimental investigations, Renewable Energy 31 (2006) 2025–2041.
[10] J.P. Bedecarrats, F. Strub, B. Falcon, J.P. Dumas, Phase-change thermal energy storage using spherical capsules: performance of a test plant, Int. J. Refrig. 19 (1996) 187–196.
[11] T. Kousksou, J.P. Bedecarrats, J.P. Dumas, A. Mimet, Dynamic modelling of the storage of an encapsulated ice tank, Appl. Thermal Eng. 25 (2005) 1534–1548.
[12] S.L. Chen, P.P. Wang, T.S. Lee, An experimental investigation of nucleation probability of supercooled water inside cylindrical capsules, Expr. Thermal Fluid Sci. 18 (1999) 299–306.
[13] S.L. Chen, C.L. Chen, C.C. Tin, T.S. Lee, M.C. Ke, An experimental investigation of cold storage in an encapsulated thermal storage tank, Expr. Thermal Fluid Sci. 23 (2000) 133–144.
[14] K. Cho, S.H. Choi, Thermal characteristics of paraffin in a spherical capsule during freezing and melting processes, Int J. Heat Mass Trans. 43 (2000) 3183–3196.
[15] Y. Cao, A. Faghri, Performance characteristics of a thermal energy storage module: a transient PCM/forced convection conjugate analysis, Int J. Heat Mass Trans. 34 (1991) 93–101.
[16] M. Lacroix, Numerical simulation of a shell-and-tube latent heat thermal energy storage unit, Solar Energy 50 (4) (1993) 357–367.
[17] H. Ettouney, H. El-Dessouky, A. Al-Ali, Heat transfer during phase change of paraffin wax stored in spherical shells, ASME J. Sol. Energy Eng. 127 (2005) 357–365.
[18] S.V. Patankar, Numerical heat transfer and fluid flow, McGraw-Hill, New York, 1980.
[19] S.L. Lee, A strongly implicit solver for two-dimensional elliptic differential equations, Numer. Heat Transfer 16 (1989) 161–178.
[20] J. Doormaal, G.D. Raithby, Enhancements of the SIMPLE method for predicting incompressible flow problem, Numer. Heat Transfer 7 (1984) 147–158.
[21] D. Kunii, M. Suzuki, Particle-to-fluid heat and mass transfer in packed beds of fine particles, Int. J. Heat Mass Transfer 10 (1967) 845–852.
[22] N. Wakao, S. Kaguei, T. Funazkri, Effect of fluid dispersion coefficient on particle-to-fluid heat transfer coefficient in packed beds: correlation of Nusselt numbers, Chem. Eng. Sci. 34 (1979) 325–336.